PCCP

PAPER

View Article Online
View Journal | View Issue

Cite this: *Phys. Chem. Chem. Phys.*, 2019, **21**, 22569

Distinct ionic adsorption sites in defective Prussian blue: a 3D-RISM study†

Nirun Ruankaew, [ab] Norio Yoshida, [b] Yoshihiro Watanabe, [b] Akira Nakayama, [c] Haruyuki Nakano [b] and Saree Phongphanphanee *[adef]

Received 6th August 2019,
Accepted 20th September 2019

DOI: 10.1039/c9cp04355a

rsc.li/pccp

Ferric hexacyanoferrate (FeHCF) or Prussian blue (PB) exhibits selective alkali ion adsorption and has great potential for use in various applications. In the present work, alkali ion (Li^+, Na^+, K^+, and Cs^+) and water configurations in defective PB (d-PB) were studied by using the statistical mechanics of molecular liquids. The three-dimensional (3D) distribution functions of the ions and water were determined by solving the 3D-reference interaction site model (RISM) equation of systems of a unit lattice of d-PB in electrolyte solutions, *i.e.*, LiCl, NaCl, KCl, and CsCl. The results show the difference in the ion–water configurations and distributions between small (Li^+ and Na^+) and large ions (K^+ and Cs^+). The adsorption sites of Li^+ and Na^+ are located off-center and lie on the diagonal axis. By contrast, the larger ions, K^+ and Cs^+, are adsorbed at the center of the unit cell. The degree of dehydration due to the adsorption of alkali ions indicates that there was no water exchange during Li^+ and Na^+ adsorption, whereas two and three water molecules were removed after adsorption of K^+ or Cs^+ in the unit cell.

Introduction

Prussian blue (PB) or ferric hexacyanoferrate (FeHCF) is a well-known dark-blue dye pigment that has been widely used in painting since the classical period.[1,2] In the past few decades, PB has been considered a promising material in various fields of science,[3–5] medicinal materials,[2,6] environmental materials and battery technology.[7–12] The demand for Li-ion batteries has dramatically increased with the rapid growth in portable electronic devices, electric automobiles, service robotics, and solar energy storage. PB and its analogue compounds (PBAs) have a number of fascinating properties, as well as the fact that they are environmentally friendly, their synthesis is inexpensive, and they have a high adsorption capacity and selectivity specific to alkali ions.[13–15] In particular, they have good potential as cathode materials for alkali ion batteries.[11,16,17] The ionic selectivity of PB and PBA depends on the size of the ions, with large ions being preferred over small ones.[18–21] PB and PBAs are also attractive materials for application in high-activity sorbents for the removal of hazardous radioactive metal contamination. A number of recent experiments show the high adsorption capacity of composites between PB and other materials, such as core–shell nanoparticles, polymer nanocomposites and thin film layers.[3,4,15,21–24]

The crystal and chemical structure of PB were investigated by various techniques, such as X-ray powder diffraction,[25] X-ray diffraction,[26,27] polarized neutron diffraction,[28,29] and neutron scattering.[30] Its chemical formula was reported as $Fe_4[Fe(CN)_6]_3{\cdot}xH_2O$ (x = 14–16).[26] For all PBA compounds in the hexacyanometallate family, the generic formula can be written as $M'_x[M(CN)_6]_y{\cdot}zH_2O$, where M and M′ represent transition metal ions with charge 2+ and 3+, respectively, and are coordinated octahedrally with C and N atoms of the cyano ligand. The crystallographic studies mentioned above concluded that PB has a face-centered cubic structure of type $Fm\bar{3}m$, with a lattice constant α = 10.166 Å. However, the cubic structure and lattice constant of PBA can vary according to the atomic size of the transition metal ions. The d-PB structure can occur when the $[Fe^{II}(CN)_6]^{4-}$ or $[M(CN)_6]^{4-}$ group is missing, allowing the creation of a spherical cavity at the center of the lattice, corners, or surfaces. In this defective structure, the particular compound stoichiometry (x/y ratio from the generic formula) is larger than one while this number is equal to one for perfect PB (p-PB).[30,31]

[a] *Department of Materials Science, Faculty of Science, Kasetsart University, Bangkok 10900, Thailand. E-mail: fscisrph@ku.ac.th*
[b] *Department of Chemistry, Graduate School of Science, Kyushu University, Fukuoka 819-0395, Japan*
[c] *Department of Chemical System Engineering, Graduate School of Engineering, The University of Tokyo, Tokyo 113-8656, Japan*
[d] *Computational Biomodelling Laboratory for Agricultural Science and Technology, Faculty of Science, Kasetsart University, Bangkok 10900, Thailand*
[e] *Specialized center of Rubber and Polymer Materials in Agriculture and Industry, Faculty of Science, Kasetsart University, Bangkok, 10900, Thailand*
[f] *Thailand Center of Excellence in Physics (ThEP Center), Commission on Higher Education, Bangkok 10400, Thailand*

† Electronic supplementary information (ESI) available. See DOI: 10.1039/c9cp04355a

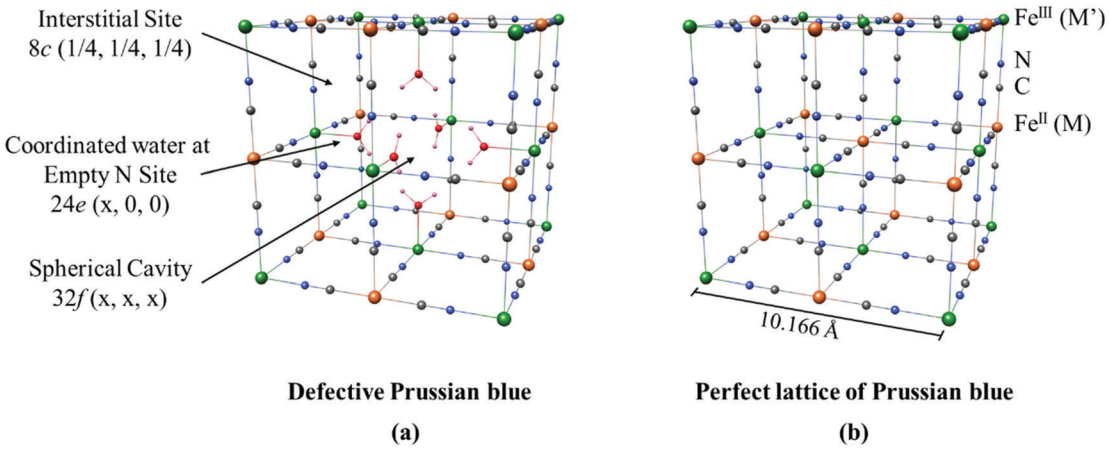

Fig. 1 Schematic illustration of the Wyckoff crystallographic position of (a) d-PB ($Fe^{III}_4[Fe^{II}(CN)_6]_3{\cdot}xH_2O$) in comparison to (b) a lattice of p-PB ($Fe^{III}_4[Fe^{II}(CN)_6]_4{\cdot}xH_2O$). The connection between O_w and 24e Fe^{III} in d-PB is added as a guide for the eye. The letters M and M′ stand for transition metal ions in PBA compounds. The water positioned at the 32f spherical cavity and in 8c interstitial sites in both structures was omitted for better vision.

The structures of p-PB and the central vacancy in d-PB with the Wyckoff positions are shown in Fig. 1. In 1977, Buser *et al.* prepared single crystals of PB for their X-ray investigation by reacting $FeCl_2{\cdot}4H_2O$ with $K_4Fe(CN)_6{\cdot}3H_2O$, and $FeCl_3{\cdot}6H_2O$ with $H_4Fe(CN)_6$.[26] Their X-ray studies revealed that PB was approximately 18% in the form of p-PB, with a 73% probability that the central $Fe^{II}(CN)_6$ group would be missing, and only a 9% chance of it being in other positions such as a surface or a lattice corner site. Nowadays, the chemical synthesis of PB has developed, and the ratio of d-PB per p-PB can be adjusted depending on the starting materials, synthesis method and post-synthesis modification.[24] The different structures of p-PB and d-PB would lead to different properties of the materials. Our recent work demonstrated that hydrated p-PB contains an average of 7.4 zeolitic water molecules, with each such molecule located at an interstitial site of the subunit.[19] However, in d-PB, the lack of the octahedral $[Fe^{II}(CN)_6]^{4-}$ creates a center cavity, which contains more water molecules. This could be the cause of the larger number of water molecules, 14–16, detected in PB by experiments.[26,27,32] The water inside p- and d-PB plays an important role in ion intercalation and controls the redox process.[5] Wu *et al.* reported that the coordinated and zeolitic water in d-PB prohibits Na from intercalation, and suggested that p-PB has a greater ion capacity than d-PB for Na-ion battery technology.[9,10] The water structure inside d-PB was confirmed by the neutron diffraction study of Herren *et al.*[29] and the neutron scattering study of Sharma *et al.*[30] They suggested that there are three kinds of water sites in a d-PB lattice, namely, the coordinated water molecules at 24e empty N sites, and the non-coordinated ones in the 32f spherical cavity and at 8c interstitial sites (see Fig. 1). By contrast, p-PB has only non-coordinated water molecules (zeolitic water) at 8c interstitial sites. PBs are capable of adsorbing alkaline, alkali, and some small organic cations in aqueous solution.[33] It has been hypothesized that the adsorption mechanism of PB occurs *via* ion–ion and ion–water exchange processes depending on the structure of PB.[18,19,26,34] In 2014, Ishizaki *et al.* proposed that Cs^+ is adsorbed into d-PB's spherical cavity sites by chemical adsorption with proton exchange; the mechanism occurs with an acidic environment.[35,36]

Recently, we investigated the adsorption site of alkali ions in p-PB by using a statistical mechanics theory of liquids, called the "three-dimensional (3D)-reference interaction site model (RISM)". Our results show distinct adsorption sites between small ions (Li^+ and Na^+) and large ions (K^+ and Cs^+). Moreover, we calculated the number and configuration of water molecules around and inside p- and d-PB. The results demonstrated that at least one water molecule is located at the 8c interstitial site of p-PB[19] and approximately 14 water molecules are located in different positions inside d-PB,[37] in accordance with the experimental studies of Herren *et al.*[29] and Sharma *et al.*[30] Despite there are a number of studies on selective ion adsorption and transportation through PB, the mechanisms remain to be clarified; for example, the dehydration number and its configuration after ions are intercalated into d-PB still have inconsistent conclusions. The dehydration numbers of PBA compound, such as nickel hexacyanoferrate (NiHCF), intercalated by Cs^+ were reported as two and three water molecules.[18,21,38] Also, the results of intercalation of Na^+ into NiHCF are in conflict; for instance, Yu *et al.*[21] reported that there was no water molecule exchange while Lasky and Buttry[38] showed that 0.5 or at least one molecule was expelled after Na^+ was intercalated. Moreover, to our knowledge, there are no reports on the number of dehydration when FeHCF is the host material for ion intercalation.

This work is devoted to the solvation of alkali ions in d-PB and to the number of exchange water molecules during the intercalating process. The 3D-RISM method was applied to investigate the 3D-distribution functions (DFs) of the Li^+, Na^+, K^+ and Cs^+ ion and water configurations inside the unit cell of d-PB which lacks the central hexacyanoferrate. It should be noted that we focus on d-PB with a central vacancy, while defects on the other sites of d-PB are not included in this study. To analyze the solvation of an ion in d-PB, an explicit ion was applied to the adsorption site and then the 3D-DFs of the

solvent were calculated. The results could indicate the adsorption sites of the ions, and their solvation structure in d-PB.

Computational method

To obtain the ion and water distribution, we considered a single unit of d-PB that was missing the central hexacyanoferrate as a solute, which was taken from X-ray crystallography of Buser *et al.*[26] The bond lengths between atoms in Fe^{II}–C, Fe^{III}–N, and C–N are 1.923, 2.029, and 1.131 Å, respectively. To fulfill the Fe coordination complex structure, we added cyanide ligands onto the surface of the subunit lattice site except at the 24e empty N site (see Fig. S1 in the ESI†), these ligands were removed before performing the 3D-RISM calculation. All the water molecules were treated as the ''solvent'' in the 3D-RISM calculations.

To assign the partial atomic charge on the solute, the electrostatic potential charges were obtained from the CHELPG fitting method[39] at the DFT level, using the Becke three-parameter, Lee–Yang–Parr (B3LYP) exchange–correlation functional.[40,41] The effective core potential of Hay and Wadt (LANL2DZ) was used for the frozen inner-core electrons (1s, 2s, and 2p orbitals) of all Fe atoms,[42,43] and the 6-31G(d) basis set was applied for all C and N atoms of the cyanide ligands.[44–47] The DFT calculations were performed as single-point energy calculations without geometry optimization, and the spin multiplicity of mixed-valence Fe was 21, as suggested by Schulte and Frank.[48] All DFT calculations in this study were performed using the Gaussian 09 Revision E.01 program package.[49] The atomic coordinates and ESP charges of each atom are explicitly listed in Table S1 in the ESI.†

The 12-6 Lennard-Jones parameters, ε_i and σ_i, of each d-PB atom were taken from the unified force field[21,50] (see Table 1 in ref. 19). The water and ions of aqueous solutions of LiCl, NaCl, KCl, and CsCl were described by SPC and OPLS parameters, respectively (see Table 2 in ref. 19). The solvent–solvent correlation functions of the electrolyte solutions were obtained by dielectrically consistent RISM (DRISM).[51,52] The concentration, temperature, and dielectric constant in the DRISM calculations were 0.1 M, 298 K, and 78.5, respectively. The number of grids in the calculations was 8192 and the width was 0.02 Å. The d-PB lattice was individually subjected to the electrolyte solutions at infinite dilution. Then, the 3D-RISM equation[53] was solved coupled with the Kovalenko–Hirata closure equation (KH closure).[54,55] The box size in all 3D-RISM calculations was $64 \times 64 \times 64$ Å^3 with a spacing of 0.25 Å, which created $256 \times 256 \times 256$ grid points. The potential parameters of the explicit ions were the same as those in the implicit ion calculation. For the explicit ion calculations, we used bulk water as a medium to investigate ion solvation in d-PB. The numerical tolerance for DRISM was 1×10^8 and for 3D-RISM was 1×10^6. The DRISM and 3D-RISM calculations were performed using in-house software.[56] We have checked that the box size is sufficient to meet charge neutrality of the system by integrating the charge density of ions. The total net charge of d-PB and the electrolyte solutions in the calculation box is −12.7 and 12.6, respectively, so charge neutrality is certainly satisfied.

Results and discussion

Ions in bulk solutions

The selective adsorption of ions into the materials from aqueous solution was analyzed by comparing the solvated structure of ions in bulk water and in the materials. We performed 3D-RISM to obtain the solvation structure of each ion, *i.e.*, Li^+, Na^+, K^+, and Cs^+, in a bulk water environment. The radial pair distribution functions (RDFs) between the cations and the oxygen of water (O_w) in bulk water are shown in Fig. S2 in the ESI.† The first maximum positions of the RDFs corresponding to the first solvation shell were at 2.1, 2.4, 2.9, and 3.3 Å for Li^+, Na^+, K^+, and Cs^+, respectively; this was in good agreement with previous experimental and simulation results.[57,58] The water coordination number (cn) of an ion was calculated by integrating the RDF of water from the center of the ion into the first solvation shell,

$$\mathrm{cn} = 4\pi\rho\int_0^b g(r)r^2\mathrm{d}r \quad (1)$$

where ρ and b are the water density and the radial distance of the first minimum of the RDF, respectively. We found that in bulk solution, Li^+, Na^+, K^+, and Cs^+ were coordinated by 3.91, 4.39, 5.12, and 6.68 water molecules, respectively, which fall within the range reported in the literature.[59–61] It should also be noted that the first solvation shell and the cn of the ions were in accordance with the ionic sizes.

Water distribution inside d-PB

Fig. 2(a) illustrates the isosurface plot of the 3D distribution function (3D-DF) of O_w in d-PB with $g_{O_w}(\mathbf{r}) = 5$. The term $g_{O_w}(\mathbf{r}) = 5$ in this context means that the probability to find O_w at position $\mathbf{r}$ is five times greater than that in the bulk; this term also applies to all the other solvent species in our calculation for the following discussion.[62] The 3D-DF of O_w demonstrates the high distribution of water at the 24e empty N sites, and 8c interstitial sites, and a broad peak at the 32f spherical cavity site can be observed at $g_{O_w}(\mathbf{r}) < 5$. The contour plots for the 3D-DF of O_w are depicted in Fig. 2(b and c); the contour planes pass through the isosurface on the (002) and (004) plane, as defined in Fig. 2(a). The results from the contour plot on the (002) plane show four strong peaks at the 24e empty N sites. These four strong peaks represent the solid water coordinated to Fe^{III} at the sites. The angular averaging of the 3D-DF of O_w inside the unit cell around 24e Fe^{III} (Fig. 3) shows the distance between Fe^{III} and O_w at the 24e empty N sites to be 2.13 Å, which is in good agreement with experiments.[27,32] In the same plane, the contour plot also exhibits a broad peak at the center of the d-PB lattice; this peak represents non-coordinated water, which is related to the high probability of finding a water molecule in the region of the 32f spherical cavity. The contour plot on the (004) plane and its virtual image on the (00−4) plane show moderate heights for four peaks (eight in total) (Fig. 2(c)); these peaks represent another type of non-coordinated water in the d-PB lattice, which is located at the 8c interstitial sites. Besides these four peaks, we can observe another strong peak of coordinated water on the

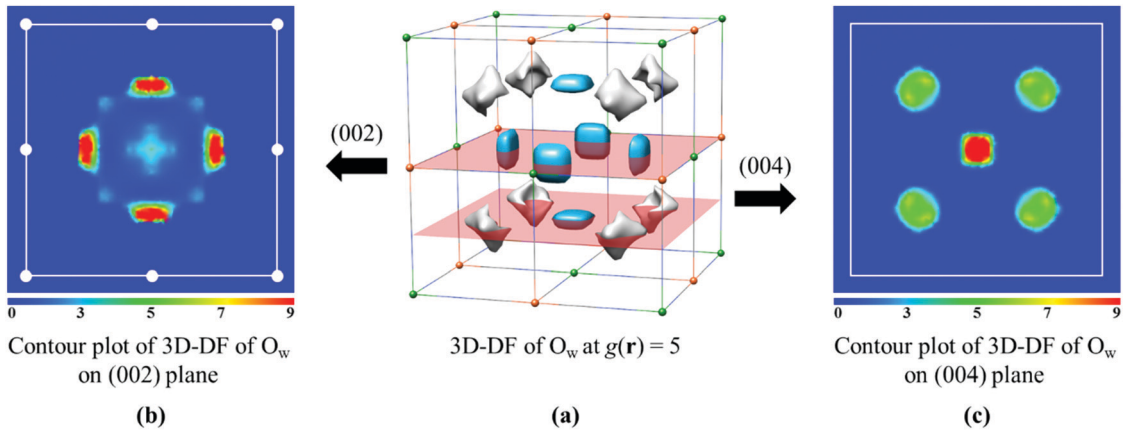

Fig. 2 (a) An isosurface plot of the 3D-DFs of O_w when $g(\mathbf{r}) = 5$. The distributions around the 8c interstitial site and the 24e empty N site are colored gray and blue, respectively. (b and c) Contour plots of the 3D-DF of O_w on the (002) and (004) planes, respectively. The white squares represent the area inside the d-PB lattice where the planes (transparent red) pass through, and the white circles represent all the $Fe^{II/III}$ ions located on the (002) plane.

(004) and (00−4) planes. These water site positions, 24e, 8c, and 32f, are consistent with the experimental results of Herren *et al.*[29] and Sharma *et al.*[30] The number of water molecules in the d-PB system was calculated by integrating eqn (1), and is summarized in Table 1. We found that 14.05 water molecules were distributed in d-PB, which indicated that there were six coordinated water molecules at the 24e empty N site, eight non-coordinated ones at the 8c interstitial site, and others inside the 32f spherical cavity site of d-PB.

Ion distribution in d-PB

In this part, we discuss the distributions of ions in d-PB. It is noted that 3D-RISM/KH tends to underestimate the peak heights and the cn of ions.[63] However, the theory well reproduces the peak position of ions compared with the experimental data.[62,64]

The 3D-DFs of ions inside d-PB are shown in Fig. 4. The 3D-DFs of Li^+ and Na^+ showed similar patterns, with their highest peak appearing to shift slightly toward the 8c interstitial site and align on the diagonal axis. We could not observe a distribution greater than 8 at the center of the 32f spherical cavity site. In p-PB, the peaks of the distribution of Li^+ and Na^+ appeared at the channel entrance or window,[19] however, these peaks disappeared in this study (Fig. 4(a and b)).

Regarding the larger ions, the 3D-DFs of K^+ and Cs^+ showed a shape different from that of smaller ions. The distribution peaks of the 3D-DF of K^+ appeared at two sites: the first high distribution was on the diagonal axis, the same as Li^+ and Na^+ (Fig. 4(a and b)), and the other high peak of K^+ was located at the most central site of the d-PB unit cell. However, Cs^+ was distributed only at the center site. These results reveal the different adsorption sites between small and large ions.

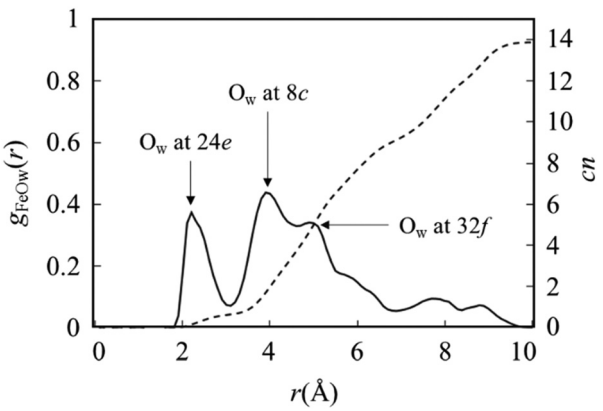

Fig. 3 RDF between 24e Fe^{III} and all 14 of the O_w inside the d-PB lattice (full line) and its cn (dashed line). The highest peaks of the first, second, and third solvation shells appear at 2.13, 4.04, and 5.08 Å, respectively.

Explicit ions and solvation structure

Solvated structure of explicit Li^+ and Na^+. To determine the water coordination to ions inside d-PB, we calculated the 3D-DFs of water in a d-PB system with an explicit ion, Li^+ or Na^+, located at the highest distribution position (Fig. 5(a)). The RDF of water with respect to the explicit ion was calculated by angular averaging of the 3D-DF, and the coordination number (cn) of each explicit ion was calculated by integrating the RDF (Fig. 6(b)). The results indicated that the ion is solvated by tetrahedral water molecules; Li^+ and Na^+ are coordinated with three water molecules from the 24e empty N site and one water molecule from the 8c interstitial site (Fig. 5(a)). The RDFs of ion–water demonstrate that the positions of the first peak of g_{LiO_w} and g_{NaO_w} inside d-PB are the same as those of g_{LiO_w} and g_{NaO_w} of the bulk solution (Fig. 6(a and b)). This demonstrates that the hydrated ion in PB has the same size as that in bulk solution.

The number of water molecules in d-PB with an explicit ion is 13.87 for Li^+ and 13.39 for Na^+, while that without an explicit ion is 14.05. This indicates that d-PB adsorbs Li^+ without water–ion exchange, which is similar to Li^+ adsorption in p-PB. Our finding is consistent with the experimental studies in the literature[18,34,38] that there is no water lost when the small ions, Li^+ or Na^+, are adsorbed into d-PB.

Solvated structure of explicit Cs^+. The 3D-DF of water with explicit Cs^+ was the most characteristic; it showed one sharp

Table 1 Overall water molecules in the d-PB structure with and without one explicit ion, and a comparison of the degree of dehydration between FeHCF ($Fe_4[Fe(CN)_6]_3{\cdot}xH_2O$) and NiHCF ($Ni_4[Fe(CN)_6]_3{\cdot}xH_2O$)

		Degree of dehydration	
Structure	Overall (3D-RISM)	FeHCF (3D-RISM)	NiHCF (ref.)
d-PB without explicit ions	14.05 (ref $\approx$ 14)[26,27,29]	—	—
d-PB with explicit Li	13.87	0.18	N/A
d-PB with explicit Na	13.39	0.66	0[21]–0.5[38]
d-PB with explicit K	12.29[c] 12.79[i]	1.76[c] 1.26[i]	N/A
d-PB with explicit Cs	10.76	3.29	2.7[21]–3.2[38]

[i]Explicit K^+ at 8c interstitial sites. [c]Explicit K^+ at the 32f spherical cavity.

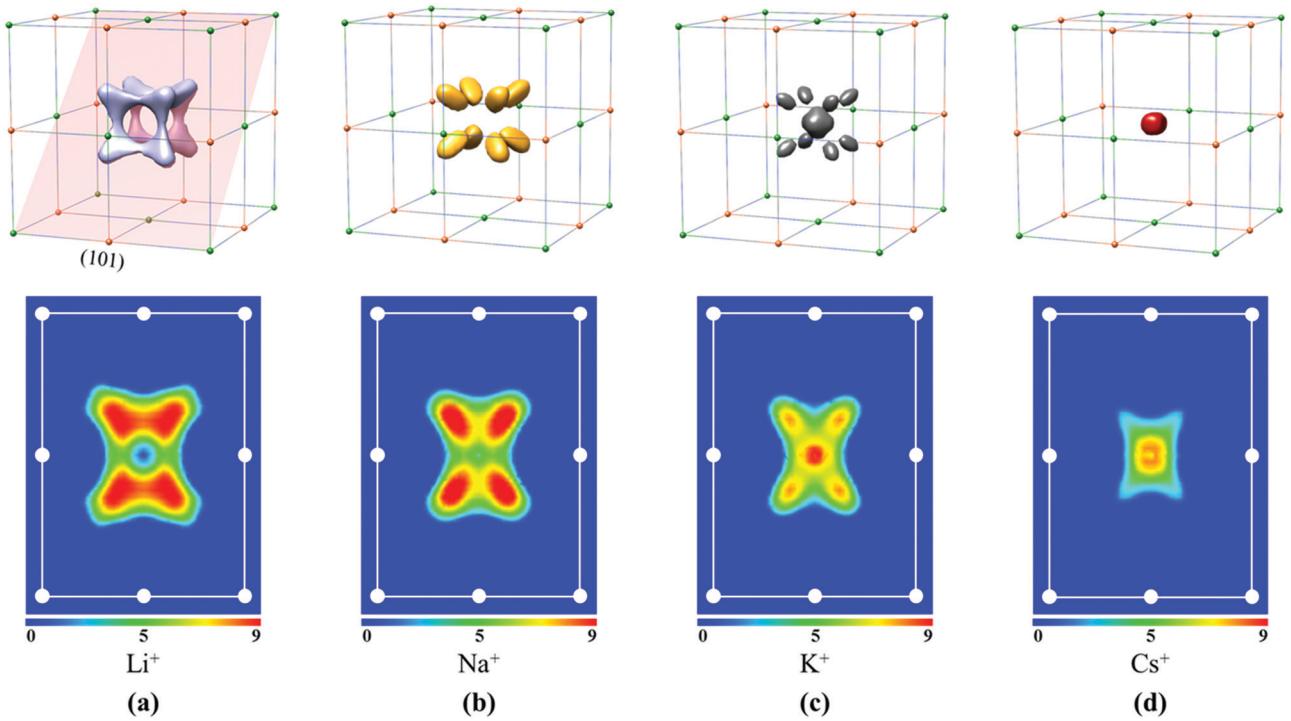

Fig. 4 (Top) Isosurface plots of the 3D-DF of (a) Li^+ and (b) Na^+ at $g(\mathbf{r})$ = 8, and (c) K^+ and (d) Cs^+ at $g(\mathbf{r})$ = 7 inside d-PB. (bottom) Contour plots of the 3D-DF of O_w on the (101) plane of each ion species. The white rectangle represents the area inside the d-PB lattice where the (101) plane (transparent red) passes through, and the white circles represent all the $Fe^{II/III}$ ions located on the (101) plane.

peak only at the most central 32f spherical cavity, indicating that the Cs^+ site is located at the central vacancy of $Fe^{II}(CN)_6$ (Fig. 4(d)). The RDF between O_w and Cs^+ in d-PB is compared with the bulk solution in Fig. 6(d). The first peak of g_{CsO_w} in the d-PB system shows a slight shift toward the center, which means that the hydrated Cs^+ in d-PB is slightly smaller than that in the bulk solution. Moreover, the water coordination number of the explicit Cs^+ in d-PB indicates that the Cs^+ ion is solvated by six water molecules in an octahedral molecular geometry (Fig. 5(b)). These solvated water molecules are located at the 24e empty N site crystallography position in d-PB, and form a bridge between Cs^+ and 24e Fe^{III}. For the ion–water exchange mechanism for Cs^+ adsorption, the results from the experiments as well as some simulations suggested that the number of dehydration during Cs^+ intercalation was approximately 2.7−3.2 molecules.[21,38] Comparing the number of water molecules in the implicit and explicit ion models (Table 1) indicates that 3.29 water molecules are lost when Cs^+ is adsorbed at the center site in d-PB.

Solvated structure of explicit K^+. As mentioned above, the distribution of K^+ inside d-PB was different from the other ions. The peaks of the 3D-DF of K^+ appeared in two positions: the first appeared toward the 8*c* interstitial site, similar to the smaller ions, and the second appeared sharply at the center site of the 32f spherical cavity, similar to Cs^+. To analyze the solvated structures, we placed an explicit K^+ at both positions separately and calculated the 3D-DF of water by solving the 3D-RISM equation. For convenience in the discussion, the positions of the explicit K^+ were defined as K_i^+ for K^+ located toward the 8c interstitial site, and K_c^+ for K^+ located at the

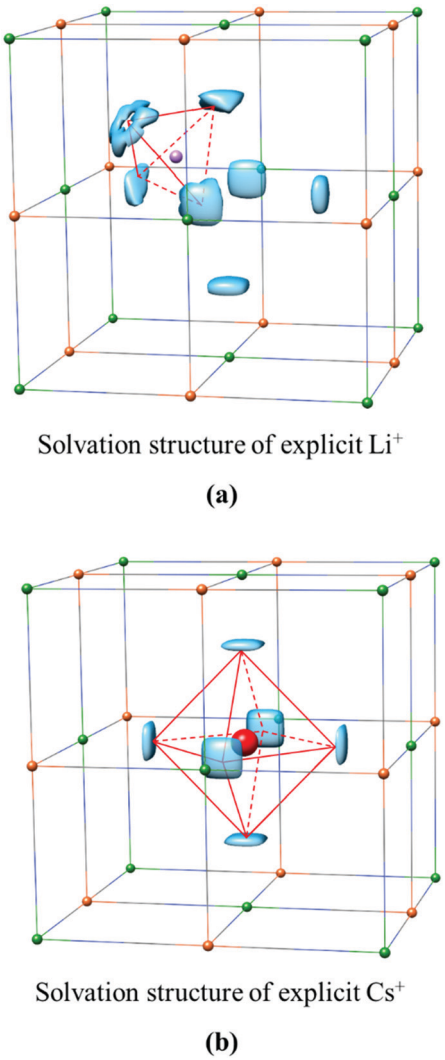

Fig. 5 Isosurface plots of the 3D-DF of O_w when (a) Li^+ and (b) Cs^+ were placed as explicit ions. The red line illustrates the tetrahedral molecular geometry of the solvation structure of Li^+ and the octahedral molecular geometry of the solvation structure of Cs^+ by water.

center of the 32f spherical cavity. The 3D-DF and RDFs of water around both explicit K^+ are shown in Fig. 6(c). The RDF of water around K_c^+ illustrates a pattern similar to that of the explicit Cs^+: the peak is located at the same position as Cs^+. This indicates that the hydrated K^+ and Cs^+ have the same size, which might be caused by the strong coordination of water to Fe, restricting the position of water molecules. Furthermore, the coordinated water number of K_c^+ was the same as that of explicit Cs^+. Regarding the K_i^+ position, the value of g_{KiOw} showed that the distance between O_w and K_i^+ was shorter than that of K_c^+; likewise, cn significantly dropped from six to four molecules. The numbers of water molecules inside d-PB with explicit K_c^+ and K_i^+ were 12.29 and 12.79, respectively. Therefore, the number of exchanged water molecules after K^+ adsorption was in the range of 1.26–1.76 molecules. We also calculated the free energies of explicit K^+ in each position and found that the free energy for explicit K_i^+ was -14.80 kcal mol^{-1}, whereas that

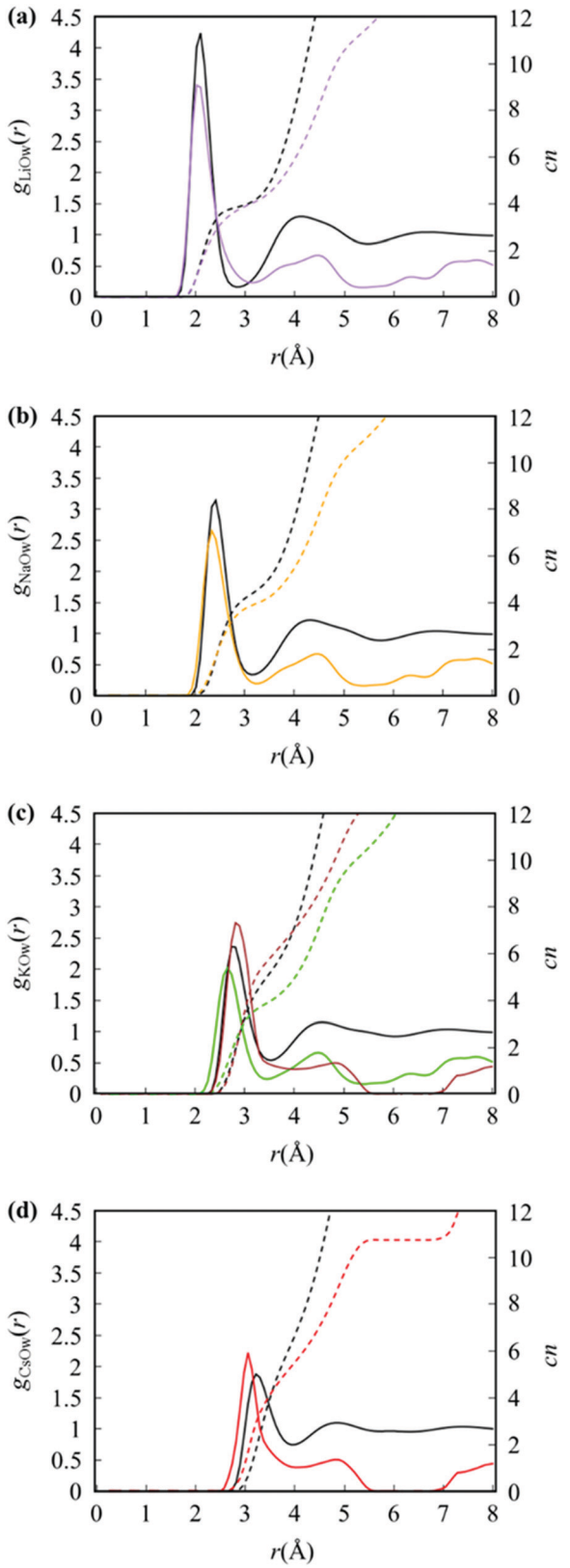

Fig. 6 RDF between O_w and explicit (a) Li^+ (pink), (b) Na^+ (orange), (c) K_i^+ (green), (c) K_c^+ (brown) and (d) Cs^+ (red) that were placed inside d-PB. The black full lines are the RDFs between O_w and ions in bulk solution. The cn of each explicit ion (colored dashed line) in d-PB and the bulk solution (black) are shown by dashed lines.

for explicit K_c^+ was −22.49 kcal mol^{-1}. This indicated that K^+ was more energetically favorable at the 32f spherical cavity site of d-PB, which is in accordance with the 3D-DF of the implicit ion.

Conclusions

We performed 3D-RISM calculations to analyze the ion–water configuration inside d-PB. The 3D-DF results showed that the small ions, Li^+ and Na^+, are adsorbed by d-PB at sites close to the interstitial site. As for the larger ions, K^+ and Cs^+, their adsorption sites are located at the center of the spherical cavity of d-PB. Moreover, we also found that adsorbed Li^+ is solvated by four water molecules and forms a tetrahedral geometry with the three 24e coordinated water molecules and one zeolitic water from the 8c interstitial site. By contrast, the larger ions, K^+ and Cs^+, would be solvated by only six 24e coordinated water molecules when they are adsorbed into d-PB. We calculated the degree of dehydration when one ion was intercalated in d-PB and compared this with the NiHCF structure studied by other theoretical methods and experiments. Our calculations indicated that the small ions can be intercalated into d-PB without losing water, whereas the large ions expel approximately three water molecules when penetrating the d-PB structure.

We believe that our results are of benefit for advancing the understanding of the mechanism underlying selective ion adsorption in PB, which is important for improving the electrochemical process and designing new materials effective for removing hazardous radioactive metals from contaminated water.

Conflicts of interest

There are no conflicts to declare.

Acknowledgements

This work was supported by the Kasetsart University Research and Development Institute (KURDI), and Thailand Research fund (No. TRG5780291). NY acknowledges support from Grants-in-Aid (No. 16H00842, 16K05519, 18K05036, and 19H02677) from the Ministry of Education, Culture, Sports, Science and Tech- nology (MEXT), Japan, and the Toyota RIKEN Scholar Program at the Toyota Physical and Chemical Research Institute. Molecular graphics images were produced using the UCSF Chimera package.[65]

References

1 A. Kraft and others, *Bull. Hist. Chem.*, 2008, **33**, 61–67.
2 H. A. Hoffman, L. Chakrabarti, M. F. Dumont, A. D. Sandler and R. Fernandes, *RSC Adv.*, 2014, **4**, 29729.
3 J.-G. Wang, Z. Zhang, X. Zhang, X. Yin, X. Li, X. Liu, F. Kang and B. Wei, *Nano Energy*, 2017, **39**, 647–653.
4 A. K. Vipin, B. Hu and B. Fugetsu, *J. Hazard. Mater.*, 2013, **258–259**, 93–101.
5 P. R. Bueno, F. F. Ferreira, D. Giménez-Romero, G. Oliveira Setti, R. C. Faria, C. Gabrielli, H. Perrot, J. J. Garcia-Jareño and F. Vicente, *J. Phys. Chem. C*, 2008, **112**, 13264–13271.
6 FDA, FDA approves first new drug application for treatment of radiation contamination due to cesium or thallium, 2003.
7 X. Sun, V. Duffort and L. F. Nazar, *Adv. Sci.*, 2016, **3**, 1600044.
8 D. Su, A. McDonagh, S.-Z. Qiao and G. Wang, *Adv. Mater.*, 2017, **29**, 1604007.
9 X. Wu, M. Sun, S. Guo, J. Qian, Y. Liu, Y. Cao, X. Ai and H. Yang, *ChemNanoMat*, 2015, **1**, 188–193.
10 X. Wu, Y. Luo, M. Sun, J. Qian, Y. Cao, X. Ai and H. Yang, *Nano Energy*, 2015, **13**, 117–123.
11 A. Eftekhari, *J. Power Sources*, 2004, **126**, 221–228.
12 A. Paolella, C. Faure, V. Timoshevskii, S. Marras, G. Bertoni, A. Guerfi, A. Vijh, M. Armand and K. Zaghib, *J. Mater. Chem. A*, 2017, **5**, 18919–18932.
13 H. Fujita, H. Sasano, R. Miyajima and A. Sakoda, *Adsorption*, 2014, **20**, 905–915.
14 N. L. Torad, M. Hu, M. Imura, M. Naito and Y. Yamauchi, *J. Mater. Chem.*, 2012, **22**, 18261.
15 H. Yang, L. Sun, J. Zhai, H. Li, Y. Zhao and H. Yu, *J. Mater. Chem. A*, 2014, **2**, 326–332.
16 M. Omarova, A. Koishybay, N. Yesibolati, A. Mentbayeva, N. Umirov, K. Ismailov, D. Adair, M.-R. Babaa, I. Kurmanbayeva and Z. Bakenov, *Electrochim. Acta*, 2015, **184**, 58–63.
17 P. J. Kulesza and K. Doblhofer, *J. Electroanal. Chem. Interfacial Electrochem.*, 1989, **274**, 95–105.
18 S. D. Rassat, J. H. Sukamto, R. J. Orth, M. A. Lilga and R. T. Hallen, *Sep. Purif. Technol.*, 1999, **15**, 207–222.
19 N. Ruankaew, N. Yoshida, Y. Watanabe, H. Nakano and S. Phongphanphanee, *Chem. Phys. Lett.*, 2017, **684**, 117–125.
20 L. F. Schneemeyer, S. E. Spengler and D. W. Murphy, *Inorg. Chem.*, 1985, **24**, 3044–3046.
21 Q. Yu, W. A. Steen, K. M. Jeerage, S. Jiang and D. T. Schwartz, *J. Electrochem. Soc.*, 2002, **149**, E195.
22 C. Thammawong, P. Opaprakasit, P. Tangboriboonrat and P. Sreearunothai, *J. Nanopart. Res.*, 2013, **15**, 1689.
23 T. Sangvanich, V. Sukwarotwat, R. J. Wiacek, R. M. Grudzien, G. E. Fryxell, R. S. Addleman, C. Timchalk and W. Yantasee, *J. Hazard. Mater.*, 2010, **182**, 225–231.
24 T. Vincent, C. Vincent and E. Guibal, *Molecules*, 2015, **20**, 20582–20613.
25 J. F. Keggin and F. D. Miles, *Nature*, 1936, **137**, 577–578.
26 H. J. Buser, D. Schwarzenbach, W. Petter and A. Ludi, *Inorg. Chem.*, 1977, **16**, 2704–2710.
27 M. P. Shores, L. G. Beauvais and J. R. Long, *J. Am. Chem. Soc.*, 1999, **121**, 775–779.
28 P. Day, F. Herren, A. Ludi, H. U. Güdel, F. Hulliger and D. Givord, *Helv. Chim. Acta*, 1980, **63**, 148–153.
29 F. Herren, P. Fischer, A. Ludi and W. Haelg, *Inorg. Chem.*, 1980, **19**, 956–959.
30 V. K. Sharma, S. Mitra, N. Thakur, S. M. Yusuf, F. Juranyi and R. Mukhopadhyay, *J. Appl. Phys.*, 2014, **116**, 034909.
31 A. Kumar, S. M. Yusuf and L. Keller, *Phys. Rev. B: Condens. Matter Mater. Phys.*, 2005, **71**, 054414.

32 L. Samain, F. Grandjean, G. J. Long, P. Martinetto, P. Bordet and D. Strivay, *J. Phys. Chem. C*, 2013, **117**, 9693–9712.
33 A. A. Karyakin, *Electroanalysis*, 2001, **13**, 813–819.
34 J. Bácskai, K. Martinusz, E. Czirók, G. Inzelt, P. J. Kulesza and M. A. Malik, *J. Electroanal. Chem.*, 1995, **385**, 241–248.
35 M. Ishizaki, S. Akiba, A. Ohtani, Y. Hoshi, K. Ono, M. Matsuba, T. Togashi, K. Kananizuka, M. Sakamoto, A. Takahashi, T. Kawamoto, H. Tanaka, M. Watanabe, M. Arisaka, T. Nankawa and M. Kurihara, *Dalton Trans.*, 2013, **42**, 16049.
36 M. Ishizaki, H. Ando, N. Yamada, K. Tsumoto, K. Ono, H. Sutoh, T. Nakamura, Y. Nakao and M. Kurihara, *J. Mater. Chem. A*, 2019, **7**, 4777–4787.
37 N. Ruankaew, N. Yoshida and S. Phongphanphanee, *IOP Conf. Ser.: Mater. Sci. Eng.*, 2019, **526**, 12032.
38 S. J. Lasky and D. A. Buttry, *J. Am. Chem. Soc.*, 1988, **110**, 6258–6260.
39 C. M. Breneman and K. B. Wiberg, *J. Comput. Chem.*, 1990, **11**, 361–373.
40 A. D. Becke, *J. Chem. Phys.*, 1993, **98**, 5648–5652.
41 A. D. Becke, *J. Chem. Phys.*, 1993, **98**, 1372–1377.
42 C. M. Aguilar, W. B. De Almeida and W. R. Rocha, *Chem. Phys. Lett.*, 2007, **449**, 144–148.
43 P. J. Hay and W. R. Wadt, *J. Chem. Phys.*, 1985, **82**, 270–283.
44 Y. Yang, M. N. Weaver and K. M. Merz, *J. Phys. Chem. A*, 2009, **113**, 9843–9851.
45 L. E. Roy, P. J. Hay and R. L. Martin, *J. Chem. Theory Comput.*, 2008, **4**, 1029–1031.
46 G. A. Petersson, A. Bennett, T. G. Tensfeldt, M. A. Al-Laham, W. A. Shirley and J. Mantzaris, *J. Chem. Phys.*, 1988, **89**, 2193–2218.
47 G. A. Petersson and M. A. Al-Laham, *J. Chem. Phys.*, 1991, **94**, 6081–6090.
48 M. Schulte and I. Frank, *J. Phys. Chem. C*, 2011, **115**, 13560–13565.
49 M. J. Frisch, G. W. Trucks, H. B. Schlegel, G. E. Scuseria, M. A. Robb, J. R. Cheeseman, G. Scalmani, V. Barone, B. Mennucci, G. A. Petersson, H. Nakatsuji, M. Caricato, X. Li, H. P. Hratchian, A. F. Izmaylov, J. Bloino, G. Zheng, J. L. Sonnenberg, M. Hada, M. Ehara, K. Toyota, R. Fukuda, J. Hasegawa, M. Ishida, T. Nakajima, Y. Honda, O. Kitao, H. Nakai, T. Vreven, J. A. Montgomery, J. E. Peralta, F. Ogliaro, M. Bearpark, J. J. Heyd, E. Brothers, K. N. Kudin, V. N. Staroverov, R. Kobayashi, J. Normand, K. Raghavachari, A. Rendell, J. C. Burant, S. S. Iyengar, J. Tomasi, M. Cossi, N. Rega, J. M. Millam, M. Klene, J. E. Knox, J. B. Cross, V. Bakken, C. Adamo, J. Jaramillo, R. Gomperts, R. E. Stratmann, O. Yazyev, A. J. Austin, R. Cammi, C. Pomelli, J. W. Ochterski, R. L. Martin, K. Morokuma, V. G. Zakrzewski, G. A. Voth, P. Salvador, J. J. Dannenberg, S. Dapprich, A. D. Daniels, Farkas, J. B. Foresman, J. V. Ortiz, J. Cioslowski and D. J. Fox, *Gaussian 09, Revis. E.01*, Gaussian, Inc., Wallingford CT, 2013.
50 A. K. Rappe, C. J. Casewit, K. S. Colwell, W. A. Goddard and W. M. Skiff, *J. Am. Chem. Soc.*, 1992, **114**, 10024–10035.
51 J. S. Perkyns and B. Montgomery Pettitt, *Chem. Phys. Lett.*, 1992, **190**, 626–630.
52 J. Perkyns and B. M. Pettitt, *J. Chem. Phys.*, 1992, **97**, 7656–7666.
53 N. Yoshida, T. Imai, S. Phongphanphanee, A. Kovalenko and F. Hirata, *J. Phys. Chem. B*, 2009, **113**, 873–886.
54 A. Kovalenko and F. Hirata, *J. Phys. Chem. B*, 2002, **103**, 7942–7957.
55 A. Kovalenko and F. Hirata, *J. Chem. Phys.*, 2000, **112**, 10391–10402.
56 Y. Maruyama, N. Yoshida, H. Tadano, D. Takahashi, M. Sato and F. Hirata, *J. Comput. Chem.*, 2014, **35**, 1347–1355.
57 K. P. Jensen and W. L. Jorgensen, *J. Chem. Theory Comput.*, 2006, **2**, 1499–1509.
58 Y. Marcus, *J. Solution Chem.*, 1983, **12**, 271–275.
59 I. G. Tironi, R. Sperb, P. E. Smith and W. F. van Gunsteren, *J. Chem. Phys.*, 1995, **102**, 5451–5459.
60 Y. Tamura, H. Ohtaki and I. Okada, *Zeitschrift für Naturforsch. A*, 1991, **46**, 1–12.
61 S. H. Lee and J. C. Rasaiah, *J. Phys. Chem.*, 1996, **100**, 1420–1425.
62 S. Phongphanphanee, N. Yoshida, S. Oiki and F. Hirata, *J. Mol. Liq.*, 2014, **200**, 52–58.
63 D. Nikolic, N. Blinov, D. Wishart and A. Kovalenko, *J. Chem. Theory Comput.*, 2012, **8**, 3356–3372.
64 N. Yoshida, S. Phongphanphanee, Y. Maruyama, T. Imai and F. Hirata, *J. Am. Chem. Soc.*, 2006, **128**, 12042–12043.
65 E. F. Pettersen, T. D. Goddard, C. C. Huang, G. S. Couch, D. M. Greenblatt, E. C. Meng and T. E. Ferrin, *J. Comput. Chem.*, 2004, **25**, 1605–1612.

